Article

Not peer-reviewed version

Mechanically Recycled PLA Films Reinforced with Rice Husk and Carbonized Rice Husk Particles

Sergio Gonzalez-Serrud *, Ana Cristina González-Valoys, Marina Patricia Arrieta *

Posted Date: 19 March 2026

doi: 10.20944/preprints202603.1582.v1

Keywords: mechanically reprocessed PLA; rice husk waste; biochar; biocomposites

 doi:10.20944/preprints202603.1582.v1

Article

Mechanically Recycled PLA Films Reinforced with Rice Husk and Carbonized Rice Husk Particles

Sergio Gonzalez-Serrud [1,2,3,*], Ana Cristina González-Valoys [2,4,5,6] and Marina Patricia Arrieta [3,7,8,*]

[1] Department of Mechanical Engineering, Universidad Tecnológica de Panamá, Panamá City 0819-07289, Panamá
[2] Grupo de investigación en Geoquímica y Sosteniblidad (GeoAS), Panamá
[3] Departamento de Ingeniería Química Industrial y del Medio Ambiente, Escuela Técnica Superior de Ingeniros Industriales, Universidad Politécnica de Madrid ETSII-UPM, Spain
[4] Department of Civil Engineering, Universidad Tecnológica de Panamá, PanamáCity 0819-07289, Panamá
[5] Centro de Estudios Multidisciplinarios en Ciencias, Ingeniería y Tecnología (CEMCIT-AIP), Panama City 0801, Panamá
[6] Sistema Nacional de Investigación-Secretaria Nacional de Ciencia, Tecnología e Innovación (SNI-SENACYT), Clayton Ciudad del Saber Edif. 205, PanamáCity 0816-02852, Panamá
[7] Grupo de Polímeros, Caracterización y Aplicaciones (POLCA), Madrid, Spain
[8] CIME, Centro de Investigación en Materiales Estructurales de la Universidad Politécnica de Madrid, C/Profesor Aranguren 3, 28040 Madrid, Spain
* Correspondence: sergio.gonzalez5@utp.ac.pa (S.G.-S.); m.arrieta@upm.es (M.P.A.)

Abstract

This study investigates the development of mechanically reprocessed poly(lactic acid) (rPLA) films reinforced with rice husk (RH) and rice husk biochar (RHB) to evaluate their processing behavior, key functional properties, and disintegration under composting conditions. rPLA was produced from PLA through an additional processing cycle to simulate the valorization of industrial PLA waste, while composites containing 1 and 3 wt.% RH or RHB were manufactured by melt extrusion followed by compression molding process. Reprocessing increased the melt flow index and decreased intrinsic viscosity and viscosimetric molecular weight, evidencing the occurrence of chain scission during mechanical reprocessing. The addition of RH slightly restricted melt flow and promoted higher surface hydrophilicity, whereas RHB showed a filler-loading-dependent effect on melt flow and increased surface hydrophobicity at low content, consistent with its carbonized and less polar nature. Both RH and RHB promote nucleating effect, with increased crystallinity in RHB-containing films, and tensile tests showed that filler incorporation mainly reduced ductility compared with unfilled rPLA, while stiffness and strength was maintained or exhibited more moderate variations. Despite these contrasting trends in surface properties and thermo-mechanical performance, all formulations achieved complete disintegration within 21 days under composting conditions at laboratory scale level. Overall, RH and RHB provide a viable route to valorize agro-industrial residues in rPLA films and to tune structure–property relationships within circular-economy framework.

Keywords: mechanically reprocessed PLA; rice husk waste; biochar; biocomposites

1. Introduction

The increasing environmental burden of persistent petroleum-derived plastics, together with the need to reduce dependence on fossil resources, has accelerated the development of polymeric materials compatible with circular economy strategies. Within this context, polylactic acid (PLA) stands out as a bio-based and biodegradable polymer produced from renewable feedstocks such as corn starch or sugarcane, and it is biocompatible and biodegradable being currently widely adopted in biomedical applications, packaging, disposable products, etc. [1–3]. More than 40% of the global plastic production is used for packaging manufacture and the compostable character of PLA has

 doi:10.20944/preprints202603.1582.v1

generated great interest in packaging applications. However, the broader use of PLA in single use products is still limited due to its moderate thermal resistance and limited mechanical robustness, particularly under demanding service conditions [1]. Several research efforts have been focused on improving PLA mechanical resistance mainly focused on the development of composites and nanocomposites [4,5].

To reduce both the fossil dependance of plastics and the accumulation in the environment, the recently adopted European Packaging and Packaging Waste Regulation (PPWR) EU 2025/40 establishes mandatory minimum recycled content targets for plastic packaging to be achieved by 2030 [6]. Although PLA is inherently compostable, it is not exempt from these regulatory commitments. Therefore, the development of effective recycling strategies for PLA is essential to ensure its compliance with forthcoming recycled content requirements. For instance, contact-sensitive packaging made from plastics other than PET must contain a minimum of 10% post-consumer recycled material [7].

Beyond material selection, the mechanical integrity of polymeric components is strongly governed by the processing–structure–property relationship. In PLA, processing history and end-of-life pathways can significantly modify chain architecture and microstructure, ultimately affecting stiffness, strength, and failure behavior. Mechanical recycling, a key route in circularity, can promote thermo-mechanical degradation and chain scission, which may reduce molecular weight and alter rheological behavior [8]. These changes affect melt-processability and may compromise final mechanical performance. Therefore, strategies that restore or improve the mechanical response of mechanically recycled PLA (rPLA) while preserving sustainability benefits remain of high interest [9].

One interesting valorization pathway is the reprocessing of industrial PLA waste such as defective plastics parts discarded from the production line, production scraps, burrs, etc. as they are of a well-known origin and composition, ensuring consistency in PLA grade [10]. Moreover, as they have not entered conventional post-consumer waste streams, they typically do not require complex sorting and intensive washing steps, unlike post-consumer PLA waste [10,11], thereby facilitating a homogeneous and food-grade material as well as a more efficient and economically viable recycling processes [10].

A promising approach to increase the mechanical properties of the materials is the development of PLA-based biocomposites reinforced with agricultural by-products, which can reduce the amount of PLA in the formulation and valorize waste streams, lessen the environmental footprint [12]. In this context, rice is one of the most widely produced and consumed staple crops worldwide, and rice husk (RH) is an abundant lignocellulosic by-product generated by the rice milling industry with low cost and wide availability in rice producing countries. Meanwhile, rice husk biochar (RHB) is its carbonized counterpart with distinct surface chemistry and thermal stability [1,3]. The biochar derived from carbonized rice husk (RHB) has been recognized for its ability to improve soil quality, primarily due to its content of essential nutrients such as nitrogen. This element plays a crucial role in soil fertility, facilitating nutrient availability to plants and enhancing the soil's water retention capacity. These properties contribute to the development of a more efficient and sustainable agricultural ecosystem [13].

The incorporation of RH and RHB to PLA can modify its melt flow and crystallization behavior and can also influence mechanical behavior and failure mechanisms through changes in interfacial adhesion finding a value addition to rise waste as a secondary source of material. From a structural integrity perspective, it is important to determine whether RH and RHB increase stiffness at the expense of ductility or enable a better balance between stiffness, strength, and strain-to-failure in PLA films [12].

In this study the effect of RH and RHB addition into mechanically recycled PLA films, focusing on how filler type, natural RH or Carbonized RHB, influences processing-related parameters and the resulting thermo-mechanical performance of the mechanically recycled composites was investigated. For that, PLA was reprocessed to simulate industrial PLA waste valorization throughout a mechanically recycling process by a second melt-extrusion step (rPLA) following a previous work

 doi:10.20944/preprints202603.1582.v1

[10]. The RH particles were sieved to obtain a particle size smaller than 500 µm, while RH were further converted into biochar (RHB) by pyrolysis at 450 °C. The obtained rPLA was further loaded with both untreated rice husk (RH) and biochar (RHB) in 1 and 3 wt.%. The obtained composite films were fully characterized by assessing the intrinsic viscosity, chemical structure, microstructure, tensile properties, thermal properties, together with water barrier-related properties and disintegration under controlled composting conditions at laboratory scale level. Overall, this work aims to clarify processing–structure relationships in rPLA biocomposite films reinforced with agro-industrial residues from the rice field, supporting the design of sustainable materials within circular economy frameworks.

2. Materials and Methods

2.1. Materials

Poly(lactic acid) (PLA) pellets (Ingeo™ 2003D, $M_n \approx 70{,}000$ Da, 2 wt% D-isomer) were supplied by NatureWorks LLC (Minnetonka, MN, USA). PLA utilized in this study includes both PLA and reprocessed PLA (rPLA) to simulate the valorization of industrial PLA waste. rPLA represents PLA that has undergone an additional processing cycle, simulating the valorization of defective plastic parts from the industry following a previously developed procedure [10]. The rice husk was supplied by Cooperativa Avance R.L., Los Olivos, Los Santos, Panama. The untreated rice husk (RH) particles were filtered through a 500-micron mesh. The rice husk (RH) was converted into biochar (RHB) by pyrolysis in in a fixed-bed reactor at 450 °C (heating rate: 10 °C/min) under an inert N_2 atmosphere (12 ml/min), in the absence of O_2. This optimum temperature was chosen based on previous studies indicating that biochar produced at this rate has a balanced cost-benefit [9].

The films' formulations were fabricated using 1 or 3 wt.% content of reinforcing fillers HB or RHB to assess the impact of bio-based particlas on the properties of rPLA. Each blend was processed via melt extrusion followed by compression molding in a hot press to form films, facilitating initial evaluations at low reinforcement concentrations of 1 wt.% and 3 wt.%. These filler contents allowed for the observation of significant changes in mechanical, thermal, and biodegradability properties without compromising the material's processability [11].

2.1.1. Materials Processing

The Figure 1 shows schematically the manufacturing of PLA films with the corresponding additives starting from rPLA pellet production to film manufacturing.

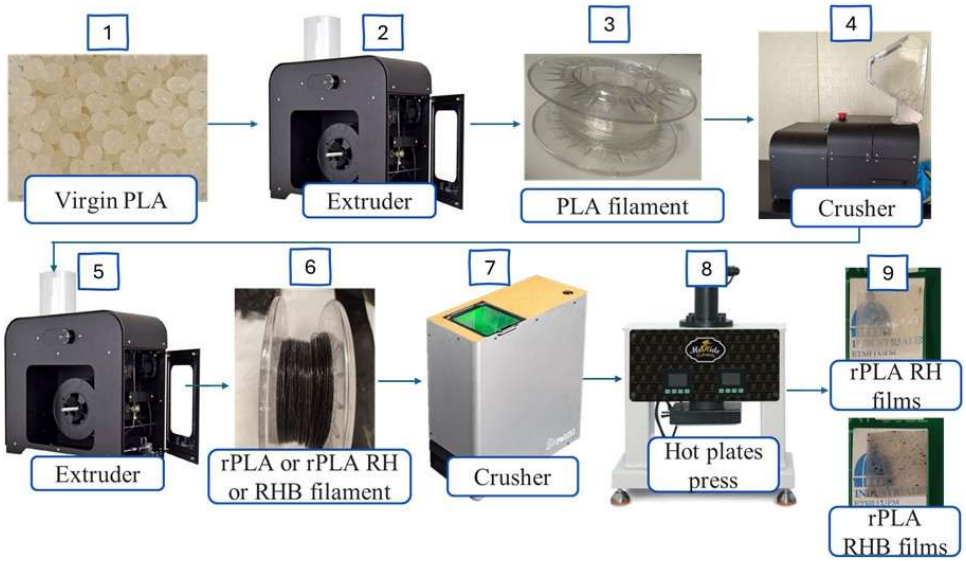

Figure 1. Methodology used to manufacture PLA, rPLA films.

 doi:10.20944/preprints202603.1582.v1

Initially, poly(lactic acid) (PLA) pellets were dried overnight at 60°C in a vacuum oven (J.P. Selecta oven, Barcelona, Spain) to prevent hydrolysis during processing. Subsequently, the PLA was processed into PLA filament. The extruder used was a 3DEVO Composer 350 extruder (3Devo, Utrecht, The Netherlands). The temperature profile along the screw, from the hopper to the nozzle, was set to 170 °C, 185 °C, 190 °C, and 170 °C, respectively, with a screw speed of 4.5 rpm. The filament was then ground into pellets by means of a Felfil Plastic Shredder+ Model 500 (Turin, Italy) to ensure a homogeneous blending with RH or RHB in the following steps.

The grounded rPLA pellets were mixed with 1 and 3 wt.% of RH or RHB, inside a sealed glass jar to ensure uniform distribution [14]. Subsequently, the mixture was introduced into the extruder and processed into composite filaments designated as rPLA-1% RH, rPLA-3%HR, rPLA-1RHB and rPLA-3%RHB. The obtained composite filament was further re-pelletized into pellets in a Felfil Plastic Shredder+ Model 500 (Turin, Italy) for further processing

2.1.2. Film Manufacturing

Previously dried rPLA pellets (60°C in a vacuum oven (J.P. Selecta oven, Barcelona, Spain) were compressed in a hot plate press to obtain the films (Mr. Hide Extracts WTRP-10T Rosin press, Tarragona, Spain). A specifically designed mold for films with dimensions of 15 x 15 cm^2 was utilized. Initially, 2g of each composite formulation was placed in the mold at 180ºC under atmospheric pressure conditions. This setup was maintained for 2 min to allow for the complete melting of the material. Subsequently, a sequential compression cycle was implemented to optimize the quality of the films and to eliminate any air bubbles potentially trapped within the material. The films were processed at a constant temperature of 180°C, under the follow pressure cycle: initially, the films were kept at atmospheric pressure for one minute, followed by the application of 3 MPa for another minute. The pressure was then increased to 5 MPa for an additional minute, and finally, 10 MPa was applied for two more minutes to ensure the removal of air bubbles from the film matrix. After compression molding process, the films were cooled to room temperature inside the plate molds under atmospheric pressure with an ice pack in contact with to ensure rapid cooling to obtain transparent films [15].

2.2. Melt Flow Index

To evaluate the melt processability of PLA, rPLA, rPLA-RH, rPLA-RHB pellets, the melt flow index (MFI) was determined using a Metrotec MFI-100 device (Techlab Systems, Lezo, Spain). The measurements were carried out at a constant temperature of 190 °C under a 2.16 kg load. For each material, six consecutive tests were performed, and each measurement was recorded over a period of 15 s.

2.2. Viscosity Molecular Weight

The intrinsic viscosity ([η]) of all the PLA-based bionanocomposite films was assessed by measuring the capillary viscosity using a Ubbelohde viscometer (type C), in compliance with ISO 1628 standards. Each sample was diluted in chloroform (Sigma-Aldrich, 99% purity) and the viscosity measurements were performed in a water bath maintained at a constant temperature of 25°C, using at least five different concentrations for each sample. Subsequently, the molecular weight of viscosity (M_v) was calculated using the Mark–Houvink equation: $[\eta] = K \times (M_v)^a$, where K and a are constants valued at $1.53x\ 10^{-2}$ and 0.759 respectively, specifically for PLA [16].

2.3. Mechanical Properties

Tensile testing was conducted at ambient temperature using an Autograph AGS-10 Series universal testing machine, which is equipped with a 100N load cell (Kyoto, Japan). The procedure adhered to the standardized protocol UNE-EN ISO 527-3. Tests were carried out on rectangular samples measuring 5 mm by 30 mm, with an initial separation of 20 mm between grips and a

 doi:10.20944/preprints202603.1582.v1

crosshead speed set at 5 mm per minute. From the stress-strain curves obtained, average values for percentage strain at break (ε_b), elastic modulus (E_t), and tensile strength (σ_t) were calculated, based on six measurements for each type of biocomposite.

2.4. Differential Scanning Calorimetry (DSC)

The thermal transitions of PLA, rPLA, rPLA 1%RH, rPLA 3%RH and rPLA 1%RHB and rPLA 3%RHB produced in this study were evaluated using differential scanning calorimetry (DSC). Thermograms were obtained in a SETLINE DSC from SETARAM (Caluire, France) through a three-step temperature cycle, which included an initial heating from 25°C to 200°C to remove thermal history, followed by cooling to 0°C, and a final heating to 240°C. The tests were conducted at 10°C/min in a nitrogen atmosphere at a flow rate of 30 mL/min. Samples weighing between 5 and 8 mg were analyzed in sealed 40 µL aluminum crucibles. Crystallinity (X_c) was calculated based on melting and cold crystallization enthalpies (ΔH_m andΔH_{cc}, respectively), with the reference melting enthalpy for fully crystalline PLA (ΔH_{0m}) set at 93 J/g [17].

$$Xc(\%) = \left[\frac{\Delta H_m - \Delta H_{cc}}{\Delta H_{0m} \cdot (1-w)}\right] \cdot 100\% \quad (1)$$

2.5. Thermogravimetric Analysis (TGA)

Dynamic thermogravimetric analyses were done in a TGA 2050 Thermogravimetric Analyzer, SETARAM (Caluire, France). One sample for each composite was placed in the analysis cell. Approximately 10 mg of samples were placed in a platinum pan and subjected to a heating ramp from 40 to 800 °C, at a rate of 10 °C/min, all within a nitrogen atmosphere. The sample is subjected to a constant temperature increase, while continuously measuring the weight loss or gain of the sample.

2.6. Attenuated Total Reflectance -Fourier Transform Infrared Spectroscopy (ATR-FTIR)

Fourier Transform Infrared Spectroscopy examination was conducted utilizing a 4X ATR-FTIR spectrometer manufactured by Jasco Corporation, headquartered in Hachioji, Tokyo, Japan. Absorbance measurements were performed across a wavelength span ranging from 4000 cm^{-1} to 400 cm^{-1}, employing 24 scan repetitions and a resolution of 4 cm^{-1}.

2.6. Static Contact Angle Measurements

The surface wettability of the films was evaluated through static water contact angle (WCA) measurements using a standard goniometer (Ossila BV, Leiden, The Netherlands) equipped with a camera and Ossila Software version 4.1.4. Drops of approximately 10 µL of distilled water were placed onto the film surfaces using a syringe, and around ten contact angle measurements were taken for each sample, with the films positioned randomly.

2.7. Water Absorption

The water absorption characteristics of the developed PLA bionanocomposite films were evaluated following the guidelines set forth in ISO 62-2008. For this evaluation, square specimens measuring 15 × 15 mm^2 were submerged in deionized water for 60 days at room temperature of 23 ± 1 °C. Throughout this testing period, the samples were removed from the water on a weekly basis, gently dried using an absorbent towel, and weighed using a AX125D analytical balance from (Nänikon, Switzerland), which offers an accuracy of $1x10^{-5}$ g. After each weighing, the samples were re-immersed in the deionized water. To ensure the reliability of the results, all tests were conducted in triplicate [17]. The water absorption rate was calculated using a specific formula (2):

$$\%\ water\ absorption = \frac{Mm\ \ \mathrm{Md}}{Md}\ x\ 100\ \% \quad (2)$$

Where Mm is the mass of the sample after exposure to moisture and Md is the mass of the dry sample.

 doi:10.20944/preprints202603.1582.v1

2.8. Water Vapor Transmission Rate

The water vapor transmission rate (WVTR) of the bio-based film composites was assessed using gravimetric methods, where silica gel served as the desiccant. Each film, covering an area of 10 cm^2, was placed over permeability cups containing 2 grams of silica gel. These setups were then stored in a desiccator maintained at 23 ± 1°C with a relative humidity of approximately 90%, using a saturated potassium nitrate (KNO_3) solution. The weight of each film formulation was recorded hourly over a six-hour period. The WVTR, expressed in grams per day per square centimeter, was determined using the equation where mt represents the weight of the cup at time t, m0 is the initial weight, and A is the film's exposed area. The results were adjusted to reflect a standard thickness of 100 micrometers [18].

$$WVTR = \frac{240\times(m_t - m_0)}{A\times t} \quad (3)$$

2.9. Field Emission Scanning Electron Microscopy (FESEM)

The cross-sectional morphology of the cryogenically fractured surfaces of each film sample was examined using field emission scanning electron microscopy (FESEM). Prior to analysis, the samples were frozen in liquid nitrogen (N_2) and cut to reveal the cross-section, followed by sputter-coating with a gold-palladium alloy.

2.10. Disintegration Under Composting Conditions

The decomposition of mats under composting conditions was evaluated at a laboratory scale in accordance with ISO 20200 standard. Film squares measuring 15 mm by 15 mm were placed in mesh textile bags to exposure to the compost medium and further facilitate the subsequent recovery [15]. Samples were then buried at depths of 4 to 6 cm within perforated plastic containers filled with a synthetic wet waste mixture. This mixture consisted of 10% compost (Mantillo, Spain), 30% rabbit food, 10% starch, 5% sugar, 1% urea, 4% corn oil, 40% sawdust, and was hydrated to approximately 50% water content by weight. The film samples were maintained under aerobic conditions at a temperature of 58°C and retrieved for analysis after 1, 4, 7, 9, 11, 14, 18 and 21 days to monitor the progress of disintegration. Photographs were taken of each sample upon retrieval to qualitatively assess the extent of physical breakdown over time.

3. Results and Discussions

3.1. Melt Flow Index

The melt flow index (MFI) results are presented in Figure 2. The commercial PLA pellet exhibited an MFI of 6.8 g/10 min, in line with values reported for virgin PLA grades [10]. In contrast, the reprocessed PLA (rPLA) displayed a marked increase in MFI (10.8 g/10 min), consistent with chain scission effects induced by thermal and mechanical stresses during extrusion. Similar values were obtained by Agüero et al. after subjecting PLA to 1 and 2 reprocessing cycles [19]. This increase indicates a reduction in molecular weight and melt-viscosity, phenomena widely reported in PLA subjected to multiple processing cycles [19–21].

When RH was introduced into the rPLA matrix, a partial decrease in MFI was observed: 9.15 g/10 min for 1 wt.% RH and 9.86 g/10 min for 3 wt.% RH. The presence of lignocellulosic particles may contribute to increased resistance to flow, possibly due to polymer-filler interfacial friction or fiber entanglement with polymer chains, which offsets part of the fluidity gained from reprocessing [22]. Similar values to that of for rPLA-1%RH of MFI were obtained for rPLA-3%RH. The nonlinear behavior with RH content suggests complex interactions between filler dispersion, fiber orientation, and rheological behavior at low filler loadings [23].

 doi:10.20944/preprints202603.1582.v1

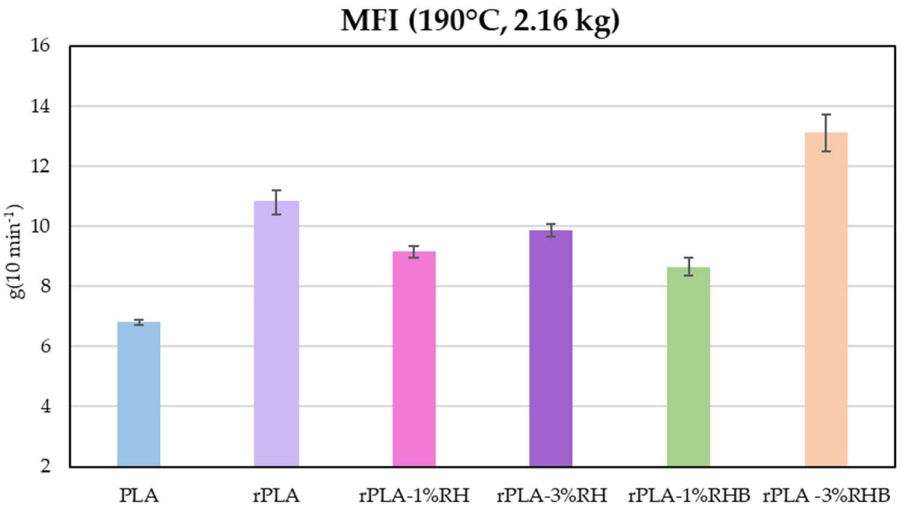

Figure 2. Determination of the melt flow index (MFI) of PLA, rPLA, and rPLA composite pellets in bulk.

Interestingly, samples reinforced with carbonized RH (RHB) exhibited different trends. At 1 wt.% RHB, the MFI further decreased to 8.64 g/10 min, reinforcing the hypothesis that RHB introduces a more pronounced barrier effect during flow, due to its more rigid, thermally stable, and porous structure, [9]. However, at 3 wt.% RHB, the MFI significantly increased to 13.1 g/10 min, surpassing even the rPLA MFI value. This sharp rise may be attributed to synergistic effects between high filler content and matrix degradation, where RHB particles, being less polar interact less with the PLA matrix, promote polymer chain slippage and reduced entanglement density, especially in matrices already weakened by thermal history. Such behavior has been previously reported in biochar-reinforced PLA systems where excessive filler loading promotes flow due to poor interfacial adhesion [24]. Additionally, biochar derived from rice husk can contain residual inorganic species (e.g., silica and mineral ash) as well as oxygen-containing surface functionalities that may act as catalytic sites under melt-processing conditions, promoting chain scission reactions in PLA during processing.

Overall, the MFI results reflect a delicate balance between matrix degradation due to reprocessing and the rheological influence of RH or RHB as fillers. While reprocessing reduces molecular weight and enhances flow, the incorporation of RH tends to moderately restrict melt mobility, whereas RHB exhibits a dual effect depending on its concentration. These findings are crucial for optimizing the extrusion conditions of rPLA-based biocomposites, especially when targeting applications requiring specific melt flow behavior.

3.2. Viscosity Molecular Weight

The Figure 3 presents the results from the viscosity molecular weight analysis of various PLA films and pellets.

The evaluation of the viscosity molecular weight (M_v) and intrinsic viscosity ([η]) of PLA and rPLA, both in pellet and film forms, reveals a clear reduction in these parameters after the material undergoes thermal processing stages (Figure 2). Specifically, the viscosity molecular weight of neat PLA pellets was 121,771 ± 1,600 g·mol^{-1}, with an intrinsic viscosity of 91.8 ± 1.5 mL·g^{-1}. In contrast, rPLA pellets exhibited lower values, with an M_v of 111,530 ± 1,100 g·mol^{-1} and an intrinsic viscosity of 88.7 ± 1.4 mL·g^{-1}, corresponding to a reduction of approximately 8.4% and 3.4%, respectively, when compared to PLA pellets. This initial decrease is indicative of the thermo-mechanical degradation suffered by the material during reprocessing cycles. The transformation of PLA into rPLA involves an additional extrusion cycle, where high temperatures and shear stress promote chain scission reactions, reducing the molecular weight of the polymer. These results are consistent with previous studies, which have reported that reprocessing of PLA leads to a gradual decrease in molecular

 doi:10.20944/preprints202603.1582.v1

weight due to the breakage of ester bonds and the formation of shorter polymer chains [25]. Further reductions in both M_v and intrinsic viscosity were observed in PLA and rPLA films. PLA films exhibited an M_v of 96,996 ± 1,500 g·mol^{-1} and an intrinsic viscosity of 81.1 ± 2 mL·g^{-1}, representing a decrease of 20.3% and 11.6%, respectively, relative to PLA pellets. Similarly, rPLA films showed an M_v of 95,830 ± 1,500 g·mol^{-1} and an intrinsic viscosity of 78.4 ± 2 mL·g^{-1}, evidencing a reduction of 14.1% and 11.7%, respectively, when compared to rPLA pellets. Similar findings were observed by Aldhafeeri et al., (2022) [20].

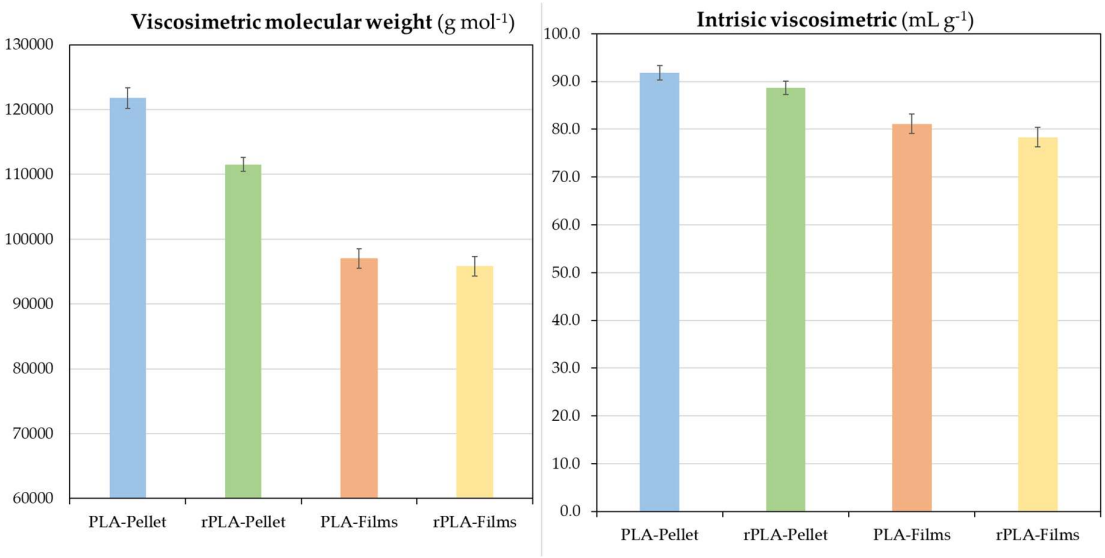

Figure 3. Viscosity molecular weight and intrinsic viscosity of PLA and rPLA-based pellets and films.

These results confirm that the extrusion and compression molding processes used for film production further accelerate the degradation of the polymer chains. The combined effect of high temperatures, shear forces, and oxygen exposure during melt processing promotes chain scission and a reduction in molecular weight, which directly influences the intrinsic viscosity of the material. This behavior is characteristic of PLA-based materials, which are susceptible to hydrolytic and thermal degradation during processing [10].

The progressive decrease on the viscosity molecular weight and intrinsic viscosity not only impacts the rheological properties of the material but also has significant implications for the mechanical and barrier performance of the films. Lower molecular weight results in reduced chain entanglement and cohesive forces within the matrix, potentially compromising tensile strength, elongation at break, and resistance to water vapor permeation [19].

From a sustainability standpoint, these findings highlight the need to control processing parameters and evaluate potential solutions, such as the incorporation of chain extenders, antioxidants, or optimized processing conditions, to mitigate the degradation of rPLA during recycling cycles. The observed reductions in molecular parameters will serve as a critical reference point to further analyze the influence of rice husk and carbonized rice husk incorporation on the physicochemical integrity and performance of the developed biocomposite films [26].

3.3. Attenuated Total Reflectance—Fourier Transform Infrared Spectroscopy (ATR-FTIR)

FTIR was used to obtain detailed information on the chemical molecular composition of the sample of RH and RHB as well as that of the composite films. The ATR-FTIR spectra of RH and RBH are summarized in Figures 7 and the ATR- FTIR spectra of all composite films are summarized in Figures 7 and 8.

 doi:10.20944/preprints202603.1582.v1

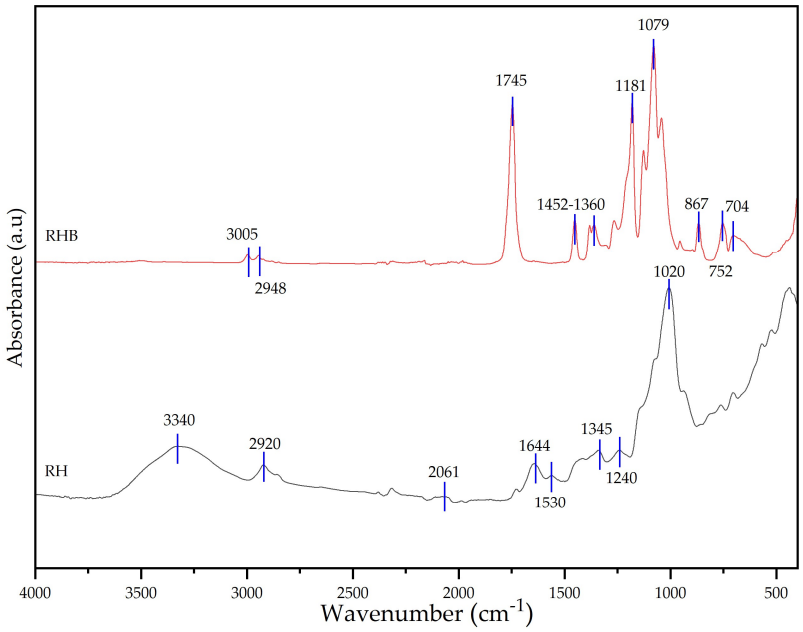

Figure 4. FTIR test on biochar rice husk (RHB) and rice husk (RH).

In the ATR-FTIR analysis of uncarbonized rice husk, a notable absorption band at 3332 cm^{-1} is evident, attributed to -OH groups, reflecting hydrogen bonds between hydroxyl groups in the glucose chains of cellulose. This band may also encompass traces of water present in the sample. Vibrational bands in the 2913 cm^{-1}, 1507 cm^{-1}, and 1369 cm^{-1} regions indicate the presence of C-H bonds, associated with aliphatic organic compounds. Around 2051 cm^{-1}, the C=O stretches from carbonyl groups in hemicellulose are observed. C-C group vibrations are found between approximately 1600 cm^{-1} and 1680 cm^{-1}, corresponding to lignin. The band around 1027 cm^{-1} is related to the stretching of the acetyl functional group, referred to as C-O. This analysis highlights the main functional groups present in the rice husk, which align with those reported in previous studies on lignocellulosic fibers [27–29].

The ATR-FTIR analysis of biochar produced from rice husk at a carbonization reveals significant insights into the chemical transformations and structural modifications that occur during the carbonization process [30]. The characteristic peaks observed in the FTIR spectrum provide valuable information about the functional groups present in the biochar and the extent of changes compared to the uncarbonized rice husk.

The peak observed at 3005 cm^{-1} corresponds to =C-H stretching vibrations, indicating the presence of alkenes or aromatic structures. This suggests that the carbonization process has facilitated the formation of aromatic rings, a key feature of biochar that contributes to its stability and potential applications [31]. The presence of a peak at 2948 cm^{-1} indicates residual C-H stretching from methylene groups, suggesting that while significant transformation has occurred, some aliphatic chains may persist in the biochar matrix. The carbonyl C=O stretching peak at 1745 cm^{-1}, although reduced in intensity, suggests that some oxygenated functional groups remain in the biochar, potentially influencing its surface reactivity. Peaks at 1452 cm^{-1} and 1382 cm^{-1} are associated with CH_2 and CH_3 bending vibrations, highlighting the presence of methyl and methylene groups that are remnants of the aliphatic structure post-carbonization [32].

The bands at 1265 cm^{-1} and 1181 cm^{-1} indicate C-O stretching vibrations in esters or ethers, suggesting that the carbonization process may preserve some structural elements from the original biomass [33]. The region encompassing 1131 cm^{-1}, 1079 cm^{-1}, and 1041 cm^{-1} reflects C-O and C-O-C stretching vibrations, consistent with ether linkages or modified cellulose remnants, demonstrating the complexity of the biochar's internal structure [32]. The band at 966 cm^{-1} may indicate =C-H

 doi:10.20944/preprints202603.1582.v1

twisting vibrations, suggesting the presence of unsaturated bonds that could result from incomplete aromatic transformation or new bond formations within the biochar matrix [28]. Finally, peaks at 867 cm^{-1}, 752 cm^{-1}, and 704 cm^{-1} are typical of out-of-plane bending vibrations in aromatic rings, confirming the development of condensed aromatic structures that are integral to the biochar's chemical stability and its potential applications [27].

Overall, the FTIR analysis highlights the transformation of rice husk into a more aromatically enriched and structurally stable material through carbonization [33]. The presence of both aromatic and aliphatic features underscores the complexity of biochar and suggests its suitability for a range of functional applications, from soil amendment to use as a filler in polymer composites [34]. This transformation aligns with existing literature, which describes biochar as a versatile material with significant potential in sustainable technologies [35].

On the other hand, the ATR-FTIR spectra of PLA film reveals several typical distinctive bands that provide insights into the polymer's chemical structure and interactions. The analysis of these FTIR bands is crucial for understanding the structural integrity and stability of PLA. The peak at 1744 cm^{-1}, attributed to the carbonyl stretching vibration of the lactide ester groups, is a prominent feature in PLA spectra [10].

The band at 1450 cm^{-1} corresponds to the bending vibrations of methyl groups (CH_3) in PLA. The C-O stretching vibrations at 1180 cm^{-1} correspond to ester linkages within PLA [36]. Additionally, the peak at 1079 cm^{-1} reflects C-O-C stretching in glycolic linkages, which are integral to the PLA backbone [2].

The spectral region between 3000 cm^{-1} and 2860 cm^{-1} is characterized by –CH stretching bands. A broad absorption around 3000 cm^{-1}, attributed to the cyclohexene group, overlaps with the –CH peaks. The spectra also exhibit the asymmetric stretching of the carbonyl group (C=O) at 1744 cm^{-1}, the CH_3 group at 1450 cm^{-1}, and symmetric and asymmetric deformation bands of –CH at 1380 cm^{-1} and 1360 cm^{-1}, respectively.

All composite films and rPLA exhibited the characteristic PLA absorption bands. No significant peak shifts or new bands were detected after reprocessing or filler addition, suggesting that the PLA main chain remained chemically unchanged within the detection limits of ATR-FTIR.

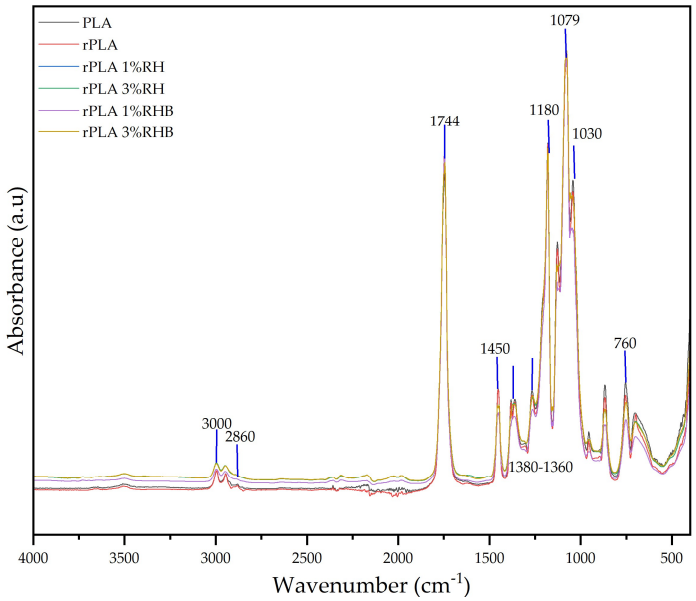

Figure 5. FTIR spectral analysis of PLA, rPLA and rPLA composite films.

 doi:10.20944/preprints202603.1582.v1

3.4. Field Emission Scanning Scanning Electron Microscopy (FESEM)

The micrographs corresponding to the cross-sectional fracture surfaces obtained by cryo-fracture by previously frozen the sample in liquid N_2 are shown in Figure 4, where the morphology of each analyzed formulation can be observed.

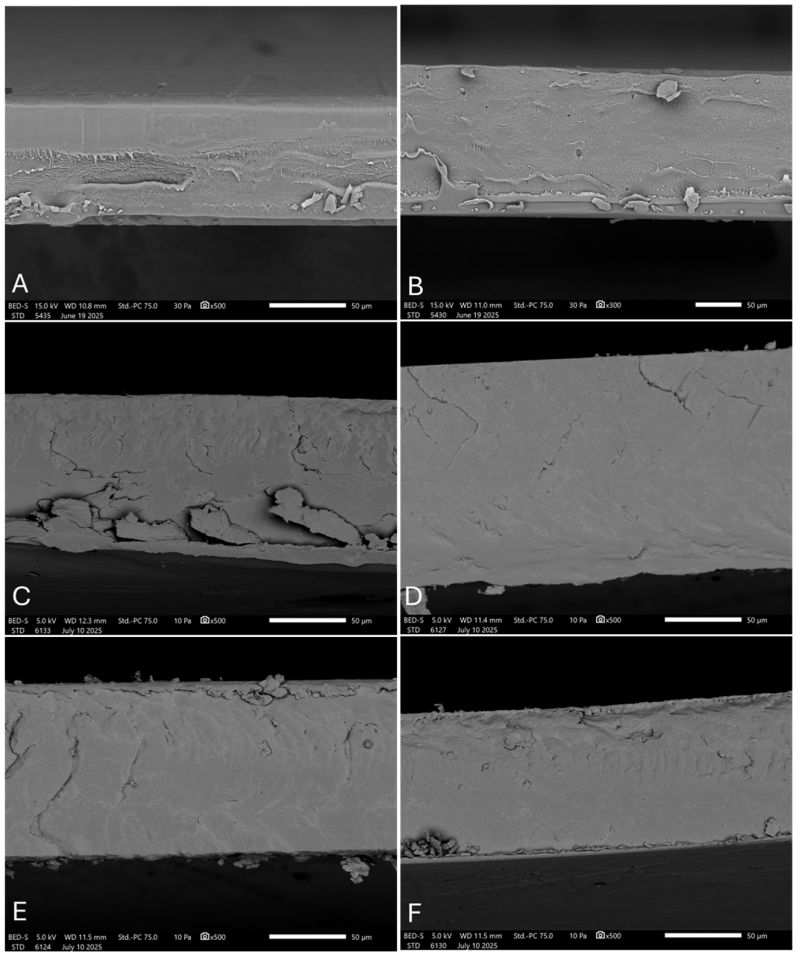

Figure 6. FE-SEM observations at films: A) PLA, B) rPLA, C) rPLA-1%RH, D) rPLA-1%RHB, E) rPLA-3%RH, F) rPLA–3%RHB.

In the PLA film (Figure 6-A), a homogeneous and continuous topography is evident, with a smooth surface and no signs of tearing. This regular morphology is characteristic of brittle fracture with minimal plastic deformation, typical of unmodified semicrystalline PLA matrices, in accordance with previous reports [10]. In contrast, the rPLA film (Figure 6-B) exhibits a visibly rougher, yet continuous fracture surface. Unlike PLA (Figure 6-A), rPLA (Figure 6-B) displays a somewhat more irregular texture attributed to the thermal degradation accumulated during the second reprocessing cycle [10,37]. For the rPLA, and RH (Figure 6-C and Figure 6-E) or RHB (Figure 6-D and Figure 6-F) loaded films, no reinforcement particles were directly observed embedded within the matrix. Similarly, no cavities, voids, or significant structural defects were identified, suggesting a good particle integration into the polymeric matrix and a reasonably homogeneous distribution, with no apparent morphological alterations compromising the structural integrity of the films [38].

3.5. Mechanical Properties

The mechanical properties of PLA and rPLA as well as the rPLA-based composites with rice husk (RH) and rice husk biochar (RHB) provide valuable insights into the impact of natural fillers on

 doi:10.20944/preprints202603.1582.v1

polymer matrices. By examining the tensile test properties, Young's modulus (E_t), tensile strength (σ_t), and elongation at break (ε_b), we can understand how these additives influence the structural and functional properties of rPLA-based materials.

The mechanical properties of PLA and rPLA-based films are summarized in figure 4. A clear decreasing trend was observed in tensile strength (σ_t), Young's modulus (E_t), and elongation at break (ε_b) as a result of reprocessing due to the thermal degradation.

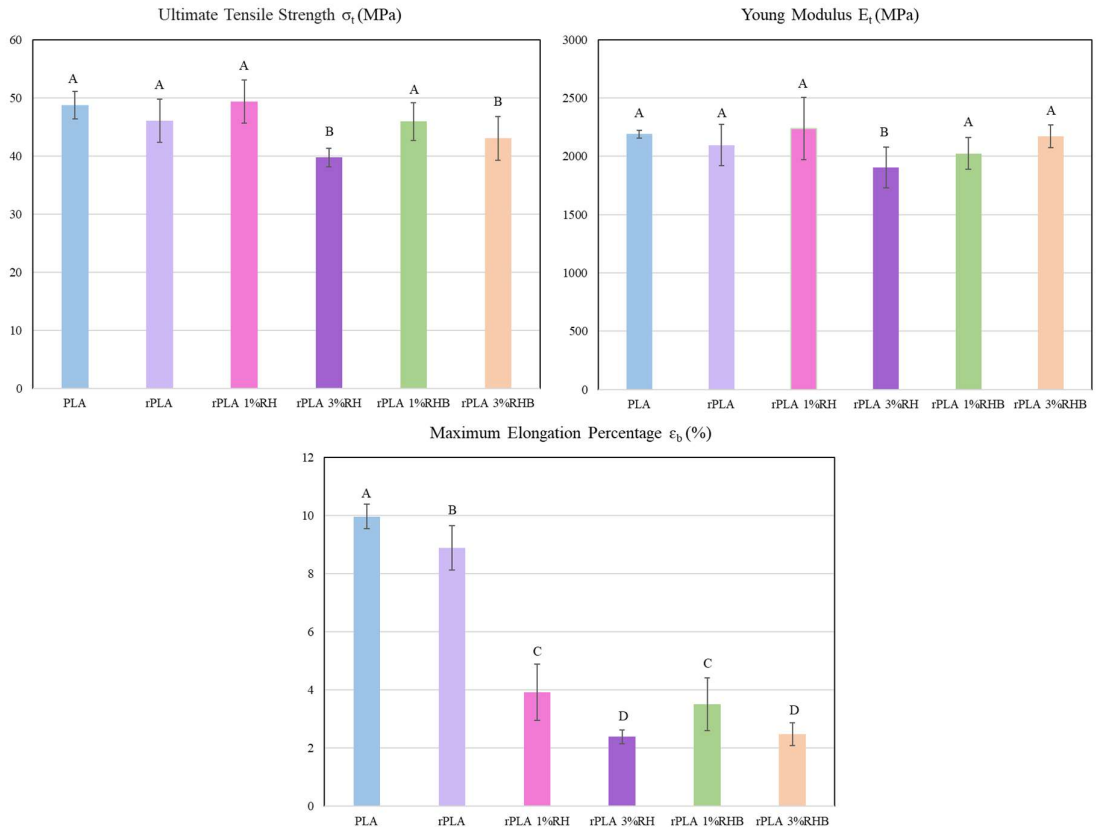

Figure 7. Tensile test of PLA, rPLA and rPLA composite films. Samples sharing at least one letter do not show significant differences, according to Fisher's least significant difference (LSD) test with $p < 0.05$, following a one-way ANOVA.

The PLA film exhibited the highest mechanical performance, with a tensile strength of 48.7 MPa, a Young's modulus of 2189.5 MPa, and an elongation at break of 10.0%. Reprocessing reduced these values to 46.1 MPa, 1954.58 MPa, and 8.63%, respectively. This decrease is associated with chain scission during reprocessing, leading to lower molecular weight and reduced chain entanglement [39].

The addition of rice husk (RH) particles further affected the mechanical behavior but in different ways according to the amount and type of rice husk-based particle. The tensile strength and modulus of rPLA-1%RH did not significantly decrease reaching values of 44.5 MPa and 1944.0 MPa, while elongation dropped significantly to 3.7%, showing a reduction in the flexibility of the films as frequently occurs in polymer composites where the particle limit plastic deformation. Increasing RH content to 3 wt.% exacerbated this effect, with tensile strength and modulus decreasing to 35.3 MPa and 1808.9 MPa, and elongation at break falling to 2.3%. The presence of 3 wt.% of RH introduced rigid, poorly adhered particles in the matrix, acting as stress concentrators and further reducing the deformation capacity [23].

The composites with carbonized rice husk (RHB) showed a more marked reduction on the overall mechanical performance than RH composites. rPLA-1%RHB exhibited a tensile strength of

 doi:10.20944/preprints202603.1582.v1

39.9 MPa, modulus of 1899.1 MPa, and elongation at break of 3%. At 3 wt.% RHB content, these values further decreased to 37.1 MPa, 1850.9 MPa, and 1.7%, respectively, which may indicate limited interfacial adhesion and inefficient stress transfer between the filler and the rPLA matrix.

3.6. Differential Scanning Calorimetry (DSC)

The DSC thermograms of all films are shown in Figure 8, while the thermal parameters obtained, including the glass transition temperature (T_g), cold crystallization temperature (T_{cc}), melting temperature (T_m), associated enthalpies (ΔH_{cc} and ΔH_m), and degree of crystallinity (X_c)are summarized in Table 2.

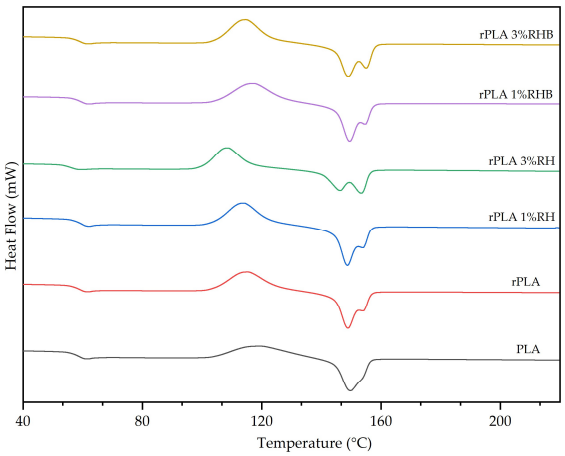

Figure 8. Differential scanning calorimetry (DSC) thermograms obtained during the second heating scan of PLA, rPLA and rPLA composite films.

Table 1. The thermal properties of poly(lactic acid) (PLA) and PLA composites reprocessed (rPLA) with rice husk (RH) and carbonized rice husk (RHB) were evaluated, including measurements of glass transition temperature (T_g), cold crystallization temperature (T_{CC}), melting temperature (T_m), cold crystallization enthalpy (ΔHCC), enthalpy of fusion (ΔHm), and degree of crystallinity (Xc).

Sample (film)	T_g (°C)	T_{cc} (°C)	T_m (°C)	ΔH_{CC} (J/g)	ΔH_m (J/g)	X_c (%)
PLA	59.0	119.9	149.7	26.	33.4	8.0
rPLA	59.2	115.2	148.9	29.1	38.4	10.0
rPLA 1%RH	59.7	114.1	148.7	29.2	35.4	6.7
rPLA 3%RH	55.9	108.5	153.4	27.5	41.0	15.0
rPLA 1%RHB	59.8	117.3	149.4	28.5	36.1	8.3
rPLA 3%RHB	59.2	114.5	149.0	29.8	44.5	16.3

The neat PLA film showed the typical behavior of PLA film, whereas the rPLA showed two melting peaks. The multimelting behavior is commonly attributed to the presence of less perfect crystals that initially melt at lower temperatures and subsequently reorganize into more stable and ordered crystalline structures, which remelt at higher temperatures, already observed in mechanically recycled PLA [40].

The T_g of the neat PLA films was 59.0 °C and remained practically constant in the reprocessed and composite formulations, with values ranging from 59.2 °C to 59.8 °C. Sepúlveda-Carter et al. reported similar T_g values of 58 °C and 58.7 °C for PLA and rPLA, respectively. [10]. An exception was observed in the rPLA-3%RH sample, where T_g decreased to 55.9 °C. This reduction may be attributed to the higher thermo-mechanical degradation in good agreement with the reduction on the molecular weight of rPLA and the marked increase in MFI values in this formulation, suggesting an increased chain mobility, while the highest content of untreated lignocellulosic fibers generate a less

 doi:10.20944/preprints202603.1582.v1

homogeneous matrix and introduce irregularities that favor increased segmental mobility in the amorphous regions of the polymer.

The T_{cc} values progressively decreased from 119.9 °C in neat PLA to 108.5 °C in rPLA-3%RH composite, indicating an enhancement of the crystallization ability in recycled materials due to the reduction in molecular weight and increased chain mobility. The addition of RH further decreases the cold crystallization temperature. This decrease of Tcc in composite can be associated with a nucleating effect induced both by reprocessing and by the addition of RH particles, promoting molecular rearrangement at lower temperatures and facilitating the crystallization of rPLA matrix during heating [41], particularly at 3 wt.% loading. The addition of 1 and 3 wt.% of carbonized particles (RHB) exhibited different tendencies. While the incorporation of 1 wt.% of RHB increase the T_{cc} values to 117.3 °C, probably due to the shorter polymer chains may become partially adsorbed onto the RHB filler surface, which can restrict their mobility and hinder their ability to reorganize into crystalline structures, which requires more thermal energy to crystallize the rPLA matrix. Meanwhile, the addition of higher content of 3 wt.% of RHB somewhat decreases the Tcc value of rPLA indicating a more homogeneous nucleating effect, probably due to their higher thermal stability of RHB and more regular surface morphology compared to RH [41].

The T_m remained stable in most formulations, with values ranging from 148.7 °C to 149.7 °C. However, a significant increase to 153.4 °C was observed in the rPLA-3%RH film sample, suggesting the formation of more stable and ordered crystals. This phenomenon may be related to recrystallization induced by the interaction between rPLA chains and RH particles associated with the formation of more stable crystalline domains, although with a lower total amount of crystals [42]. This increase in T_m was not replicated in the RHB formulations, in which the Tm values were mainly maintained, indicating differences in the nucleation mechanism and in the quality of the crystals formed depending on the nature and content of the reinforcement [14].

The melting enthalpy (ΔH_m) and cold crystallization enthalpy (ΔH_{cc}) reflect the amount of energy absorbed and released during the melting and molecular ordering processes and allows to determine the overall crystallinity in the polymeric matrix [43]. The unfilled reprocessed PLA (rPLA) showed a higher crystallinity (X_c = 10.0%) compared to neat PLA (X_c = 8.0%), which may be attributed to chain redistribution during thermal reprocessing, facilitating spontaneous nucleation during the thermal cycle [44]. The highest ΔH_m was recorded for rPLA-3%RHB (44.5 J/g), followed by rPLA-3%RH (41.0 J/g). These values suggest a general improvement in the reprocessed materials' ability to reorganize their chains and form crystalline regions, compared to PLA (33.4 J/g). Despite exhibiting a lower T_m, the rPLA 3%RHB formulation showed the highest crystallinity among all samples (X_c = 16.3%), indicating an effective nucleating action due to the synergistic effect of shorter polymer chains generated during the polymeric matrix reprocessing and RHB, possibly associated with RHB porous surface and low hygroscopicity [45]. In contrast, rPLA-3%RH, although exhibiting a higher T_m, showed slightly lower crystallinity (X_c = 15%), supporting the hypothesis that crystal perfection does not always correlate with the total amount of crystals formed [43,46].

3.7. Thermogravimetric Analysis (TGA)

Figures 9 shows the thermogravimetric curves of all films, while Table 1 compiles the data collected by the thermogravimetric analysis.

 doi:10.20944/preprints202603.1582.v1

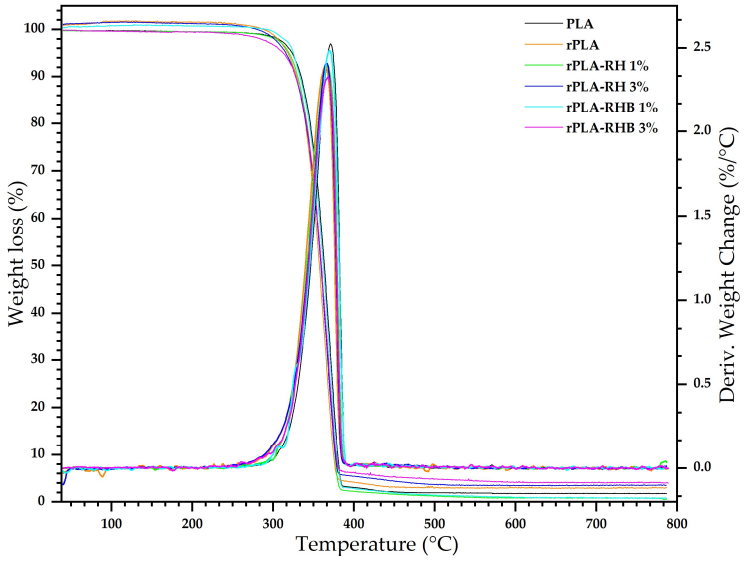

Figure 9. TGA and DTG curves of PLA, rPLA and rPLA composite films.

Table 2. Comparison of Decomposition Temperatures and Mass Loss in Different PLA Film Samples.

Sample	Initial Decomposition Temperature (°C)	Maximum Decomposition Temperature (°C)	Maximum Mass Loss Percentage
PLA	323.4	371.2	65.6
rPLA	318.2	364.7	66.2
rPLA-RH 1%	319.4	366.4	66.0
rPLA-RH 3%	315.7	366.2	57.6
rPLA-RHB 1%	325.2	369.6	65.7
rPLA-RHB 3%	312.7	368.2	66.1

PLA films exhibit a initial decomposition temperature at 323.4 °C, indicating good thermal stability for the intended use application. The maximum decomposition temperature of 371.2 °C and a maximum mass loss of 65.6% are typical characteristics of PLA, reflecting its standard thermal degradation behavior [8,10]. Upon reprocessing, a decrease in the initial decomposition temperature to 318.2 °C and a maximum decomposition temperature of 330 °C is observed in rPLA film, in good accordance with previous studies on mechanically recycled PLA [10,19,47]. This suggests that reprocessing may affect the polymers' molecular structure, likely due to thermal and mechanical degradation mechanisms. The increase in maximum mass loss to 66% could be attributed to the greater release of volatile degradation products generated during reprocessing [10,19].

The addition of 1 wt.% of rice husk (RH) to rPLA results in a slight decrease in the initial decomposition temperature to 319.4 °C and in the maximum decomposition temperature to 366.4 °C. The reduction in maximum mass loss to 66% may indicate some level of interaction between the PLA matrix and the filler, potentially improving resistance to thermal decomposition by limiting the extent of mass loss [1,43]. When increasing the RH content to 3 wt.%, a further reduction in both the initial (315.7 °C) and maximum (366.2 °C) decomposition temperatures is observed. This trend suggests that higher RH content may serve as degradation initiation sites due to their complex chemical nature. However, the lower maximum mass loss of 57.6% implies that RH might also contribute to some degree of thermal stabilization, possibly through char formation or barrier effects [2,48,49].

The incorporation of 1 wt.% of carbonized rice husk (RHB) yields an initial decomposition temperature of 325.2 °C, slightly higher than that of rPLA and rPLA-RH, and a reduced maximum decomposition temperature of 369.6 °C. The maximum mass loss remains at 65.7%, indicating that while carbonized RH does not significantly impact mass loss compared to RH, it may alter the degradation pathway [24]. When the RHB content is increased to 3 wt.%, the initial decomposition

 doi:10.20944/preprints202603.1582.v1

temperature decreases to 312.7 °C, and the maximum decomposition temperature drops further to 368.2 °C. Despite this decrease in thermal stability, the maximum mass loss remains at 66.1%, similar to that of non-carbonized RH system. This suggests that carbonized husk affects the onset of degradation more markedly but does not significantly influence the final degradation extent [50].

3.8. Water Contact Angle

The surface wettability of the developed films was evaluated through static water contact angle (WCA) measurements according to ASTM D5946-17. The results (Figure 9) revealed clear variations in surface hydrophilicity as a function of the polymer matrix type and the nature of the added fillers.

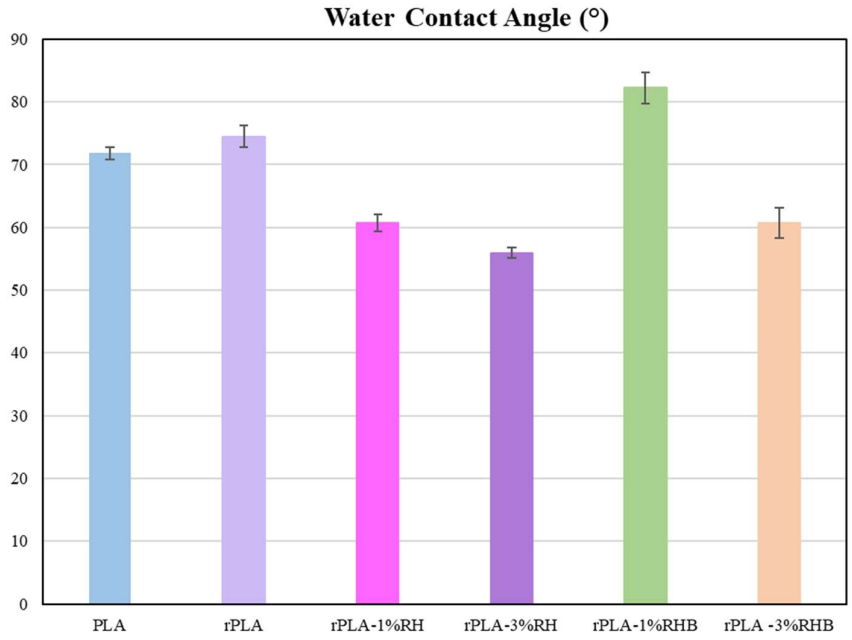

Figure 10. Static water contact angle of PLA, rPLA and rPLA composites films.

The PLA exhibited an average WCA of 71.8 ± 1.0°, which falls within the characteristic range reported for untreated PLA films (60–80°) [10,51]. This value indicates moderate hydrophilic behavior, attributed to the presence of polar carbonyl and ester groups capable of forming hydrogen bonds with water molecules [10]. The slight variability in the values reported by different authors has been associated with differences in crystallinity, surface roughness, and molecular orientation [10,25].

After reprocessing (rPLA), the WCA of rPLA film increased to 74.5 ± 1.7°, suggesting a reduction in wettability and a somewhat increase in surface hydrophobicity. This effect can be explained by molecular rearrangements and increased surface crystallinity induced during thermal reprocessing, which reduces the exposure of polar groups [25].

The incorporation of lignocellulosic rice husk (RH) particles led to a marked decrease in contact angle, with values of 60.7 ± 1.4° for 1 wt.% and 56.0 ± 0.9° for 3 wt.%. This trend indicates a progressive increase in surface hydrophilicity, attributed to the polar nature of rice husk, which is rich in hydroxyl and carboxyl groups that favor water interaction [11]. Moreover, the addition of RH particles increases surface roughness and interfacial heterogeneity, promoting water spreading [52]. Similar trends have been reported in PLA-based biocomposites reinforced with plant fibers or lignocellulosic nanoparticles, where the incorporation of hydrophilic materials decreases the WCA and enhances surface wettability [11].

In contrast, the addition of rice husk biochar (RHB) at 1 wt.% loading levels resulted in a significant increase in the contact angle (82.3 ± 2.5°), reflecting a more hydrophobic surface. This

 doi:10.20944/preprints202603.1582.v1

behavior is attributed to the carbonaceous nature and low polarity of biochar, since carbonization removes most of the hydrophilic components of biomass (cellulose, hemicellulose) and generates an aromatic surface with few oxygenated groups [53]. These characteristics reduce the surface energy and consequently the affinity of water for the rPLA-RHB-based film surface. Comparable results have been reported in PLA composites containing biochar or activated carbon, in which the contact angle can exceed 80° [53,54]. However, increasing the biochar content to 3 wt.% caused an abrupt decrease in WCA to 60.8 ± 2.4°, suggesting an exposure of polar groups at the film surface. At higher concentrations, biochar agglomerates can introduce topographical irregularities and surface defects that enhance local water retention and reduce the water contact angle value [11,14]. Additionally, this result is in good agreement with the reduction on MFI value in this formulation, that suggests thermal degradation. The formation of additional polar end groups (–COOH and –OH) associated with degradation, together with increased surface roughness caused by RHB agglomeration promotes a surface wettability increment, despite the intrinsically hydrophobic character of biochar. This non-linear behavior confirms that the hydrophobicity induced by carbon-based fillers strongly depends on their dispersion, loading, and surface functionalization [53].

Overall, the results demonstrate that the wettability of rPLA films can be tuned through the incorporation of natural or carbonized reinforcements, controlling the balance between chemical polarity and surface topography. The formulations containing RH exhibited more hydrophilic surfaces, suitable for applications requiring adhesion or compatibility with polar matrices; whereas the rPLA-1%RHB formulation showed enhanced hydrophobicity, which may be advantageous for packaging or water-resistant material applications [55].

3.9. Water Absorption

The Figure 11 presents the results of the water absorption test, which provides crucial information about the materials' ability to retain moisture under specific conditions. These results are essential for evaluating the suitability of the composites in applications where water exposure is a determining factor.

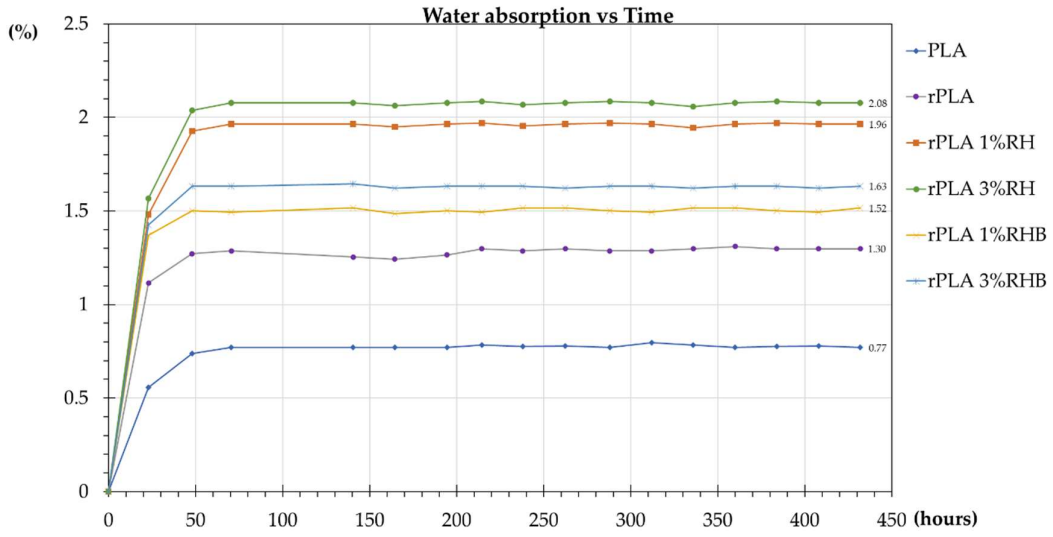

Figure 11. Water Absorption of PLA, rPLA and rPLA composite films.

PLA exhibits the lowest water absorption rates throughout the test duration, indicating its inherent hydrophobic properties. The absorption rate stabilizes around 0.77% after 70.5 hours, showing very limited increase thereafter. rPLA film shows slightly higher water absorption rates than neat PLA, which might be due to structural compromises caused by the recycling process, making it slightly more susceptible to moisture uptake. These results were similar to those reported in previous studies by [14,56,57].

 doi:10.20944/preprints202603.1582.v1

Both rPLA-1%RH and rPLA-3%RH composites show a progressively higher water absorption rate compared to rPLA counterpart, with 3 wt.% RH content the composite shows the highest absorption, reaching up to around 2.08%. This increase is likely due to the hydrophilic nature of cellulose found in rice husks, which absorbs water more readily than the PLA matrix [56,58].

rPLA with 1 wt.% and 3wt.% of RHB also demonstrate higher water absorption rates than neat PLA and rPLA films, but generally, the rates are slightly lower than those of the RH composites. This could be attributed to the more hydrophobic nature produced by the carbonization process of the rice husk, which helps reduce the overall moisture affinity of the composite [45].

3.10. Water Vapor Transmission Rate

The Figure 12 presents the results from the water vapor transmission rate (WVTR) test, which evaluates the permeability of the PLA and rPLA films and their composites with natural fillers, rice husk (RH) and rice husk biochar (RHB).

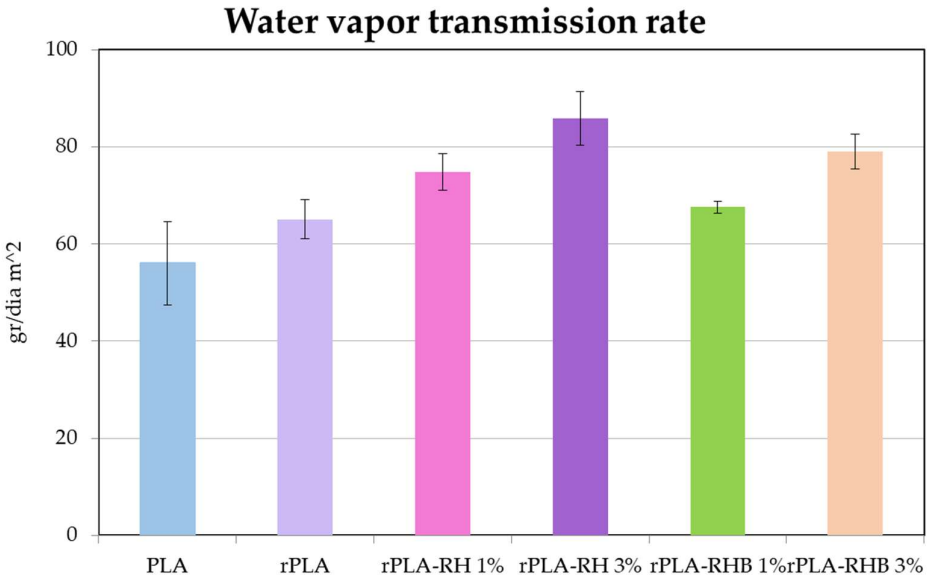

Figure 12. Water vapor transmission rate (WVTR) of PLA, rPLA and rPLA composite films.

PLA exhibits the lowest WVTR of 56.1 gr day^{-1} m^{-2}, in accordance with its hydrophobic polymer matrix and with already reported values for neat PLA [10]. rPLA film shows a higher WVTR at 65.1 gr day^{-1} m^{-2} compared to neat PLA, because of the recycling process slightly degraded the polymeric matrix reaching in shorter polymer chains that increased the polymers chain mobility, increasing its permeability to water vapor.

The rPLA-1%RH further increase the WVTR value to 74.8 gr day^{-1} m^{-2}. This indicates that the addition of RH with a hydrophilic nature facilitates the water interaction and further reducing the water barrier properties and allowing more water vapor to pass through. Accordingly, rPLA-3%RH shows a significant rise in WVTR to 85.8 gr day^{-1} m^{-2}, the highest among the samples tested. rPLA-1%RHB exhibits a WVTR of 67.6 gr day^{-1} m^{-2}, which is slightly higher than rPLA but much lower compared to RH composites. This suggests that RHB, due to its possibly more carbonized and porous structure, might interact differently with the PLA matrix, leading to a less pronounced increase in permeability. Similarly, rPLA-3%RHB records a WVTR of gr day^{-1} m^{-2}. Although this is lower than rPLA with 3 wt% RH, it's still substantially higher than the neat PLA and rPLA, indicating that higher concentrations of RHB also compromise the barrier properties but to a lesser extent than RH.

Rice husk is primarily organic and contains significant amounts of cellulose, a hydrophilic compound known to absorb moisture [2]. This characteristic naturally leads to an increase in water

 doi:10.20944/preprints202603.1582.v1

vapor transmission when used as a filler in polymer matrices such as PLA [59]. Biochar is produced through the carbonization of organic materials, such as rice husk, which increases the content of non-volatile solids and enhances its hydrophobic properties [53]. These changes make biochar less likely to absorb water compared to its untreated organic counterpart. The carbonized structure of RHB, which likely includes a network of closed and open pores, reduces its ability to interact with water molecules, thereby lowering the water vapor transmission rate in composites containing RHB [60].

3.11. Disintegration Under Composting Conditions

The disintegration ability of the composite materials under controlled composting conditions at a laboratory scale level was assessed based on the mass loss over time while buried, in accordance with the UNE EN-ISO 20200 standard. The visual changes of the unearthed film samples and the solid compost across various incubation periods are depicted in Figure 13, whereas the mass loss induced by the composting duration for all samples is presented in Figure 14.

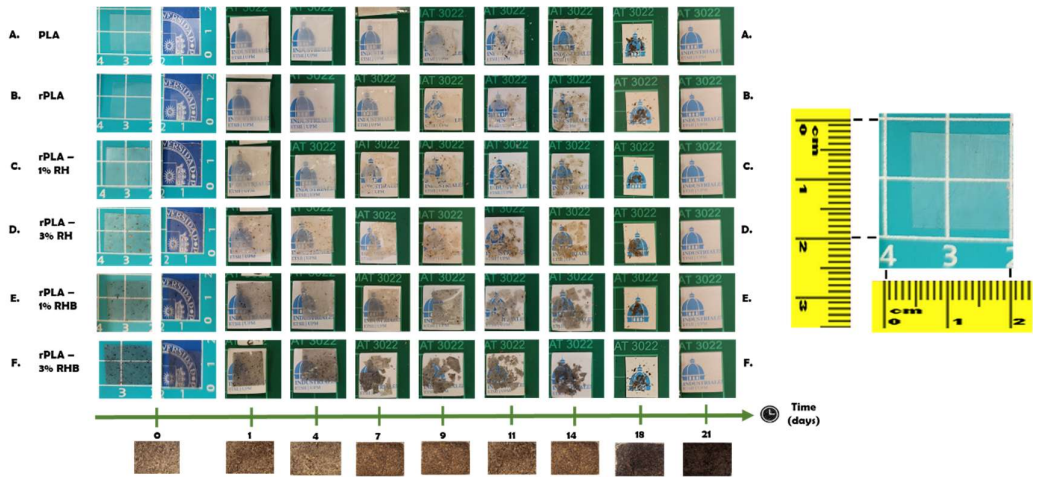

Figure 13. Evolution of the visual properties of PLA, rPLA and rPLA composite films. during compost disintegration.

From the first day of the experiment, the PLA films showed a noticeable decrease in transparency, which is indicative of the early onset of hydrolytic reactions and microbial activity facilitated by the elevated temperature (58°C) and high moisture content of the composting medium [11]. This rapid loss of transparency can be attributed to the water absorption by hydrophilic components within the film, possibly exacerbated by the presence of natural fillers like rice husk and biochar, which increases the hydrophilicity of the composite. As the degradation progressed, the films became increasingly opaque. This loss of transparency is typically associated with the physical and chemical breakdown of the PLA polymeric matrix, where the structural integrity of the films is compromised, and the material starts to exhibit visible signs of enzymatic breakdown due to microbial colonization [15]. By day 21, the films had completely disintegrated and integrated into the composting substrate. At this stage, the films lost all transparency as they broke down into smaller fragments or dissolved at the molecular level, effectively merging with the organic matter in the compost [11].

 doi:10.20944/preprints202603.1582.v1

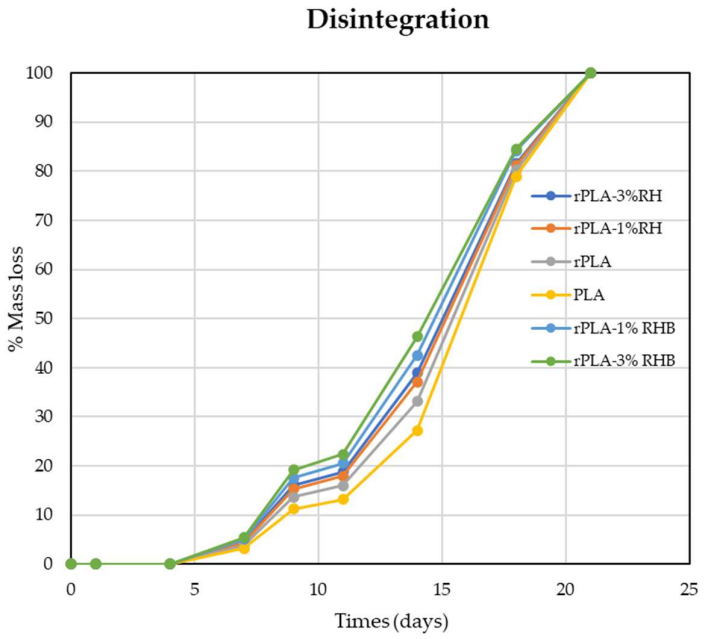

Figure 14. Disintegration curves under composting conditions.

Samples containing 3 wt.% of either RH or RHB demonstrated higher mass loss at all time points compared to those with 1 wt.% loading. This suggests that increased filler content enhances biodegradation rates, possibly due to the highest water affinity which facilitates the penetration of water and microorganisms [16,61]. Composites with RHB tended to decompose faster than those with RH throughout the entire test period. For instance, rPLA-3%RHB showed a 46.4% mass loss on day 14 and 84.6% by day 18, while rPLA-3%RH reached 38.9% on day 14 and 81.7onat day 18. Similarly, rPLA-1%RHB exhibited 42.5% on day 14 and 84.2% on day 18, outperforming rPLA-1%RH, which reached 37.1% and 81.4%, respectively.

Although PLA and rPLA showed slower disintegration, they still reached 78.9% and 80.2% mass loss by day 18. These results confirm that both the reprocessing of PLA and the incorporation of RH or RHB somewhat influence the degradation behavior [10]. The enhanced disintegration in RHB-based films may be attributed to their more porous and reactive surface chemistry resulting from carbonization [9,45]. Overall, RH and RHB enhance the disintegration rate of rPLA-based materials without compromising full disintegration by day 21, which is essential for compostable applications [58].

5. Conclusions

Although PLA is bio-based, it is considered plastic under Regulation (EU) 2025/40 and is therefore subject to mandatory recycled-content requirements for packaging from 2030. Therefore, to simulate the valorization of PLA waste from the industrial sector such as discarded defective PLA parts, plastics edges, burrs, scraps, etc. Neat PLA pellets were subjected to two extrusion process (rPLA) and then the obtained reprocessed pellets were loaded with rice husk (RH) and rice husk biochar (RHB) showing that these particles modify the processing–structure behavior relationship of mechanically reprocessed PLA (rPLA) films. Reprocessing increased melt flow and reduced intrinsic viscosity/Mv, confirming chain scission and diminished melt viscosity. Adding RH moderately reduced melt flow, whereas RHB produced a concentration-dependent response, highlighting distinct filler–matrix interactions during processing. Tensile testing revealed that the dominant mechanical effect of both fillers was embrittlement, evidenced by a pronounced reduction in elongation at break (≈1.7–3.7%) compared with PLA (~10%). While stiffness and strength were mainly maintained at low loading levels of 1 wt.%, while changed moderately, the sharp loss of ductility

 doi:10.20944/preprints202603.1582.v1

indicates that failure becomes increasingly controlled by defect sensitivity and interfacial limitations in 3 wt.% filled rPLA films. DSC showed that RH and especially RHB promoted crystallization and increased crystallinity (up to ~16%), which may contribute to the observed reduction in strain-to-failure. Wettability and water barrier properties were tunable: RH increased hydrophilicity and moisture sensitivity, whereas low RHB loading of 1 wt.% increased hydrophobicity. Despite these differences, all formulations achieved complete disintegration under composting conditions within 21 days.

Overall, the results emphasize that improving the mechanical reliability of rPLA–agro-residue films require targeted interfacial engineering (e.g., coupling agents/compatibilizers or filler surface modification) and dispersion control to mitigate embrittlement while preserving circular-economy and compostability advantages interest for single use applications such as films for food packaging or agriculture applications.

Author Contributions: Conceptualization, S.G-S. ,A.C.G-V., and M.P.A.; methodology, S.G-S ,A.C.G-V., and M.P.A.; software, S.G-S.; validation, S.G-S., A.C.G-V., and M.P.A.; formal analysis, S.G-S., and M.P.A.; investigation, S.G-S., A.C.G-V., and M.P.A.; resources, M.P.A.; data curation, S.G-S., and M.P.A.; writing—original draft preparation, S.G-S., and M.P.A.; writing—review and editing, S.G-S., and M.P.A.; visualization, S.G-S. ,A.C.G-V., and M.P.A.; supervision, M.P.A.; project administration, M.P.A.; funding acquisition, M.P.A. All authors have read and agreed to the published version of the manuscript.

Funding: This research was funded by the PID-AEI project (grant PID2024-157368NB-C32), funded by MICIU/AEI/10.13039/501100011033 and by the "ERDF A way of making Europe" as well as (MICINN) MCIN/AEI/10.13039/501100011033 through PID2021-123753NA-C32 project and by ERDF "A way of making Europe" by the "European Union" and the research consolidation project (grant CNS2022-136064) funded by MCIN/AEI/10.13039/501100011033 and by the "European Union NextGeneration EU/PRTR". S. Gonzalez acknowledge the Secretaría Nacional de Ciencia, Tecnología e Innovación (SENACYT) of the Republic of Panama for the mobility grant to Madrid.

Institutional Review Board Statement: Not applicable.

Informed Consent Statement: Not applicable.

Data Availability Statement: Not applicable.

Acknowledgments: The authors would like to thank the Secretaría Nacional de Ciencia, Tecnología e Innovación (SENACYT) of the Republic of Panama for the financial support of the project, as well as the Master's program in Mechanical Engineering of the School of Mechanical Engineering of the Technological University of Panama (UTP). The authors would like to thank the Centro de Estudios Multidisciplinarios en Ciencias, Ingeniería y Tecnología (CEMCIT-AIP) for facilitating the realization of this project. During the revision of this manuscript, the authors used ChatGPT-5.3 (OpenAI) to improve English grammar. The authors reviewed and edited the generated content as necessary and take full responsibility for the content of this publication.

Conflicts of Interest: The authors declare no conflict of interest.

References

1. Biyanti, S.K.; Hertiana, D.R.; Paramitha, T. Synthesis and Characterization of Poly-Lactic Acid (PLA) Biocomposites Reinforced with Rice Husk and Clay.; 2023; p. 090007.
2. Wu, C.S.; Tsou, C.H.; Fabrication, Characterization, and Application of Biocomposites from Poly(Lactic Acid) with Renewable Rice Husk as Reinforcement. *Journal of Polymer Research* **2019**, *26*, doi:10.1007/s10965-019-1710-z.
3. Kampeerapappun, P.; O.-Charoen, N.; Dhamvithee, P.; Jansri, E. Biocomposite Based on Polylactic Acid and Rice Straw for Food Packaging Products. *Polymers (Basel).* **2024**, *16*, 1038, doi:10.3390/polym16081038.
4. Karagöz, İ. Production and Characterization of Sustainable Biocompatible PLA/Walnut Shell Composite Materials. *Polymer Bulletin* **2024**, *81*, 11517–11537, doi:10.1007/s00289-024-05247-4.

 doi:10.20944/preprints202603.1582.v1

5. Jannatiha, N.; Gutiérrez, T.J. Recycling and Revalorization of PLA and PHA-Based Food Packaging Waste: A Review. *Sustainable Materials and Technologies* **2025**, *44*, e01364, doi:10.1016/j.susmat.2025.e01364.
6. European Union Regulation (EU) 2025/40 of the European Parliament and of the Council of 19 December 2024 on Packaging and Packaging Waste, Amending Regulation (EU) 2019/1020 and Directive (EU) 2019/904, and Repealing Directive 94/62/EC (Text with EEA Relevance). *Official Journal of the European Union, L Series* **2025**, *40*, 1–202.
7. European Union Packaging and Packaging Waste (from 2026) Available online: https://eur-lex.europa.eu/EN/legal-content/summary/packaging-and-packaging-waste-from-2026.html (accessed on 16 March 2026).
8. Silva, T.; Rodríguez-Mercado, F.; Bruna, J.E.; Torres, A.; Arrieta, M.P.; Faba, S.; Galotto, M.J.; Guarda, A.; Romero, J. Characterization of Simulated Postconsumer Recycled Poly (Lactic Acid) (<scp>PLA</Scp>): Evaluation of Reprocessing Cycles on Its Physicochemical Properties. *Journal of Polymer Science* **2025**, *63*, 2043–2054, doi:10.1002/pol.20241028.
9. Botta, C.; Grottola, C.M.; Amato, D.; Acocella, M.R. Biochar as Sustainable Filler of Recycled Polylactic Acid (PLA): A New Generation of Processable Biocomposites. *Polymers (Basel).* **2024**, *16*, 3347, doi:10.3390/polym16233347.
10. Sepúlveda-Carter, J.; Faba, S.; Rodríguez, M.S.; Arrieta, M.P. Reprocessing of Simulated Industrial PLA Waste for Food Contact Applications. *Polymers (Basel).* **2025**, *17*, doi:10.3390/polym17182439.
11. Agüero, A.; Lascano, D.; Ivorra-Martinez, J.; Gómez-Caturla, J.; Arrieta, M.P.; Balart, R. Use of Bacterial Cellulose Obtained from Kombucha Fermentation in Spent Coffee Grounds for Active Composites Based on PLA and Maleinized Linseed Oil. *Ind. Crops Prod.* **2023**, *202*, 116971, doi:10.1016/j.indcrop.2023.116971.
12. Soriano-Cuadrado, B.; Fontecha-Cámara, M.Á.; Mañas-Villar, M.; Delgado-Blanca, I.; Ramírez-Rodríguez, M.D.; Mechanical, Thermal and Morphological Study of Bio-Based PLA Composites Reinforced with Lignin-Rich Agri-Food Wastes for Their Valorization in Industry. *Polymers (Basel).* **2024**, *16*, doi:10.3390/polym16172462.
13. Tadayon, M.S.; Mousavi, S.M.; Hosseini, S.M. Salicylic Acid and Biochar-Biofertilizer Improve Soil Fertility, Drought Tolerance, and Fig Yield in a Semi-Arid Region. *J. Soil Sci. Plant Nutr.* **2025**, *25*, 7496–7510, doi:10.1007/s42729-025-02609-3.
14. Agüero, Á.; Lascano, D.; Garcia-Sanoguera, D.; Fenollar, O.; Torres-Giner, S. Valorization of Linen Processing By-Products for the Development of Injection-Molded Green Composite Pieces of Polylactide with Improved Performance. *Sustainability* **2020**, *12*, 652, doi:10.3390/su12020652.
15. Arrieta, M.P.; López, J.; Rayón, E.; Jiménez, A. Disintegrability under Composting Conditions of Plasticized PLA–PHB Blends. *Polym. Degrad. Stab.* **2014**, *108*, 307–318, doi:10.1016/j.polymdegradstab.2014.01.034.
16. Arrieta, M.; Fortunati, E.; Dominici, F.; López, J.; Kenny, J.M. Bionanocomposite Films Based on Plasticized PLA–PHB/Cellulose Nanocrystal Blends. *Carbohydr. Polym.* **2015**, *121*, 265–275.
17. Agüero, Á.; Garcia-Sanoguera, D.; Lascano, D.; Rojas-Lema, S.; Ivorra-Martinez, J.; Fenollar, O.; Torres-Giner, S. Evaluation of Different Compatibilization Strategies to Improve the Performance of Injection-Molded Green Composite Pieces Made of Polylactide Reinforced with Short Flaxseed Fibers. *Polymers (Basel).* **2020**, *12*, 821, doi:10.3390/polym12040821.
18. Trifol, J.; Marin Quintero, D.C.; Moriana, R. Pine Cone Biorefinery: Integral Valorization of Residual Biomass into Lignocellulose Nanofibrils (LCNF)-Reinforced Composites for Packaging. *ACS Sustain. Chem. Eng.* **2021**, *9*, 2180–2190, doi:10.1021/acssuschemeng.0c07687.
19. Agüero, A.; Morcillo, M. del C.; Quiles-Carrillo, L.; Balart, R.; Boronat, T.; Lascano, D.; Torres-Giner, S.; Fenollar, O. Study of the Influence of the Reprocessing Cycles on the Final Properties of Polylactide Pieces Obtained by Injection Molding. *Polymers (Basel).* **2019**, *11*, 1908, doi:10.3390/polym11121908.
20. Aldhafeeri, T.; Alotaibi, M.; Barry, C.F. Impact of Melt Processing Conditions on the Degradation of Polylactic Acid. *Polymers (Basel).* **2022**, *14*, 2790, doi:10.3390/polym14142790.
21. Velghe, I.; Buffel, B.; Vandeginste, V.; Thielemans, W.; Desplentere, F. Review on the Degradation of Poly(Lactic Acid) during Melt Processing. *Polymers (Basel).* **2023**, *15*, 2047, doi:10.3390/polym15092047.

 doi:10.20944/preprints202603.1582.v1

22. Bellon, J.; Bacoup, F.; Marais, S.; Gattin, R. PLA, PBS, and PBAT Biocomposites—Part A: Matrix–Filler Interactions with Agro-Industrial Waste Fillers (Brewer's Spent Grain, Orange Peel) and Their Influence on Thermal, Mechanical, and Water Sorption Properties. *Materials* **2025**, *18*, 3867, doi:10.3390/ma18163867.
23. Righetti, M.C.; Cinelli, P.; Mallegni, N.; Massa, C.A.; Bronco, S.; Stäbler, A.; Lazzeri, A.; Thermal, Mechanical, and Rheological Properties of Biocomposites Made of Poly(Lactic Acid) and Potato Pulp Powder. *Int. J. Mol. Sci.* **2019**, *20*, 675, doi:10.3390/ijms20030675.
24. Arrigo, R.; Bartoli, M.; Malucelli, G. Poly(Lactic Acid)–Biochar Biocomposites: Effect of Processing and Filler Content on Rheological, Thermal, and Mechanical Properties. *Polymers (Basel).* **2020**, *12*, 892, doi:10.3390/polym12040892.
25. Gálvez, J.; Correa Aguirre, J.; Hidalgo Salazar, M.; Vera Mondragón, B.; Wagner, E.; Caicedo, C. Effect of Extrusion Screw Speed and Plasticizer Proportions on the Rheological, Thermal, Mechanical, Morphological and Superficial Properties of PLA. *Polymers (Basel).* **2020**, *12*, 2111, doi:10.3390/polym12092111.
26. Fortunati, E.; Armentano, I.; Iannoni, A.; Barbale, M.; Zaccheo, S.; Scavone, M.; Visai, L.; Kenny, J.M. New Multifunctional Poly(Lactide Acid) Composites: Mechanical, Antibacterial, and Degradation Properties. *J. Appl. Polym. Sci.* **2012**, *124*, 87–98, doi:10.1002/app.35039.
27. Zou, Y.; Yang, T. Rice Husk, Rice Husk Ash and Their Applications. In *Rice Bran and Rice Bran Oil*; Elsevier, 2019; pp. 207–246.
28. Yap, S.Y.; Sreekantan, S.; Hassan, M.; Sudesh, K.; Ong, M.T. Characterization and Biodegradability of Rice Husk-Filled Polymer Composites. *Polymers (Basel).* **2020**, *13*, 104, doi:10.3390/polym13010104.
29. Rosa, S.M.L.; Santos, E.F.; Ferreira, C.A.; Nachtigall, S.M.B. Studies on the Properties of Rice-Husk-Filled-PP Composites: Effect of Maleated PP. *Materials Research* **2009**, *12*, 333–338.
30. Balasundram, V.; Ibrahim, N.; Samsudin, M.D.H.; Kasmani, R.M.; Hamid, M.K.A.; Isha, R.; Hasbullah, H. Thermogravimetric Studies on the Catalytic Pyrolysis of Rice Husk. *Chem. Eng. Trans.* **2017**, *56*, 427–432.
31. Wang, S.; Hu, Y.; Wang, Q.; Xu, S.; Lin, X.; Ji, H.; Zhang, Z. TG–FTIR–MS Analysis of the Pyrolysis of Blended Seaweed and Rice Husk. *J. Therm. Anal. Calorim.* **2016**, *126*, 1689–1702.
32. Armynah, B.; Atika; Djafar, Z.; Piarah, W.H.; Tahir, D. Analysis of Chemical and Physical Properties of Biochar from Rice Husk Biomass. *J. Phys. Conf. Ser.* **2018**, *979*, 012038, doi:10.1088/1742-6596/979/1/012038.
33. Hidayat; Rahmat, A.; Nissa, R.C.; Sukamto; Nuraini, L.; Nurtanto, M.; Ramadhani, W.S. Analysis of Rice Husk Biochar Characteristics under Different Pyrolysis Temperature. *IOP Conf. Ser. Earth Environ. Sci.* **2023**, *1201*, 012095, doi:10.1088/1755-1315/1201/1/012095.
34. Wu, W.; Yang, M.; Feng, Q.; McGrouther, K.; Wang, H.; Lu, H.; Chen, Y. Chemical Characterization of Rice Straw-Derived Biochar for Soil Amendment. *Biomass Bioenergy* **2012**, *47*, 268–276, doi:10.1016/j.biombioe.2012.09.034.
35. Nagaraju, K.; Prasad, T.N.V.K. V.; Naidu, M.V.S.; Chari, M.S.; Ramu, Y.R.; Murthy, B.R. Exploring the Benefits of Rice Husk Waste: Synthesis and Characterization of Biochar and Nanobiochar for Agricultural and Environmental Sustainability. *International Journal of Environment and Climate Change* **2023**, *13*, 715–725, doi:10.9734/ijecc/2023/v13i92292.
36. Agüero, A.; Corral Perianes, E.; Abarca de las Muelas, S.S.; Lascano, D.; de la Fuente García-Soto, M. del M.; Peltzer, M.A.; Balart, R.; Arrieta, M.P. Plasticized Mechanical Recycled PLA Films Reinforced with Microbial Cellulose Particles Obtained from Kombucha Fermented in Yerba Mate Waste. *Polymers (Basel).* **2023**, *15*, 285.
37. Nomadolo, N.; Mtibe, A.; Ofosu, O.; Mekoa, C.; Letwaba, J.; Muniyasamy, S. The Effect of Mechanical Recycling on the Thermal, Mechanical, and Chemical Properties of Poly (Butylene Adipate-Co-Terephthalate) (PBAT), Poly (Butylene Succinate) (PBS), Poly (Lactic Acid) (PLA), PBAT-PBS Blend and PBAT-TPS Biocomposite. *J. Polym. Environ.* **2024**, *32*, 2644–2659, doi:10.1007/s10924-023-03151-y.
38. Agüero, Á.; Lascano, D.; Garcia-Sanoguera, D.; Fenollar, O.; Torres-Giner, S. Valorization of Linen Processing By-Products for the Development of Injection-Molded Green Composite Pieces of Polylactide with Improved Performance. *Sustainability* **2020**, *12*, 652, doi:10.3390/su12020652.

 doi:10.20944/preprints202603.1582.v1

39. Hidalgo-Carvajal, D.; Muñoz, Á.H.; Garrido-González, J.J.; Carrasco-Gallego, R.; Alcázar Montero, V. Recycled PLA for 3D Printing: A Comparison of Recycled PLA Filaments from Waste of Different Origins after Repeated Cycles of Extrusion. *Polymers (Basel).* **2023**, *15*, 3651, doi:10.3390/polym15173651.
40. Arrieta, M.; Beltran, F.; Abarca de las Muelas, S.S.; Gaspar, G.; Sanchez Hernandez, R.; de la Orden, M.U.; Martinez Urreaga, J. Development of Tri-Layer Antioxidant Packaging Systems Based on Recycled PLA/Sodium Caseinate/Recycled PLA Reinforced with Lignocellulosic Nanoparticles Extracted from Yerba Mate Waste. *Express Polym. Lett.* **2022**, *16*, 881–900, doi:10.3144/expresspolymlett.2022.64.
41. Snowdon, M.R.; Mohanty, A.K.; Misra, M. Examination of a Biobased Carbon Nucleating Agent on Poly(Lactic Acid) Crystallization. *J. Renew. Mater.* **2017**, *5*, 94–105, doi:10.7569/JRM.2017.634134.
42. Feng, Y.; Ma, P.; Xu, P.; Wang, R.; Dong, W.; Chen, M.; Joziasse, C. The Crystallization Behavior of Poly(Lactic Acid) with Different Types of Nucleating Agents. *Int. J. Biol. Macromol.* **2018**, *106*, 955–962, doi:10.1016/j.ijbiomac.2017.08.095.
43. Llorente Uceta, M.A.; Horta Zubiaga, A. Técnicas de Caracterización de Polímeros. *Universidad Nacional de Educación a Distancia* **1991**.
44. Badia, J.D.; Strömberg, E.; Karlsson, S.; Ribes-Greus, A. Material Valorisation of Amorphous Polylactide. Influence of Thermo-Mechanical Degradation on the Morphology, Segmental Dynamics, Thermal and Mechanical Performance. *Polym. Degrad. Stab.* **2012**, *97*, 670–678, doi:10.1016/j.polymdegradstab.2011.12.019.
45. Zouari, M.; Devallance, D.B.; Marrot, L. Effect of Biochar Addition on Mechanical Properties, Thermal Stability, and Water Resistance of Hemp-Polylactic Acid (PLA) Composites. *Materials* **2022**, *15*, 2271, doi:10.3390/ma15062271.
46. Venkatram, S.; McCollum, J.; Stingelin, N.; Brettmann, B. A Close Look at Polymer Degree of Crystallinity *versus* Polymer Crystalline Quality. *Polym. Int.* **2023**, *72*, 855–860, doi:10.1002/pi.6508.
47. Ortega, Z.; Douglas, P.; Hanna, P.R.; Garrett, G.; Clarke, A.; Cunningham, E.; Suárez, L. Characterization of PLA Sheets Prepared by Stretching under Different Conditions: Influence of Reprocessing and Establishing Optimal Conditions. *Materials* **2023**, *16*, 5114, doi:10.3390/ma16145114.
48. Tsou, C.H.; Yao, W.H.; Wu, C.S.; Tsou, C.Y.; Hung, W.S.; Chen, J.C.; Guo, J.; Yuan, S.; Wen, E.; Wang, R.Y.; et al. Preparation and Characterization of Renewable Composites from Polylactide and Rice Husk for 3D Printing Applications. *Journal of Polymer Research* **2019**, *26*, doi:10.1007/s10965-019-1882-6.
49. Wang, W.; Ye, G.; Zhang, Y.; Bian, X.; Lin, P.; Dong, Y.; Hao, P.; Wang, X. Improved Hydrolytic Resistance of Polylactide Biocomposite Films Reinforced by Rice Husk before and after Accelerated Aging. *Polym. Compos.* **2025**, *46*, 590–606, doi:10.1002/pc.29010.
50. Zouari, M.; Devallance, D.B.; Marrot, L. Effect of Biochar Addition on Mechanical Properties, Thermal Stability, and Water Resistance of Hemp-Polylactic Acid (PLA) Composites. *Materials* **2022**, *15*, 2271, doi:10.3390/ma15062271.
51. Arrieta, M.; López, J.; Ferrándiz, S.; Peltzer, M. Characterization of PLA-Limonene Blends for Food Packaging Applications. *Polym. Test.* **2013**, *32*, 760–768, doi:doi.org/10.1016/j.polymertesting.2013.03.016.
52. Wenzel, R.N. Resistance of Solid Surfaces to Wetting by Water. *Ind. Eng. Chem.* **1936**, *28*, 988–994.
53. Papadopoulou, K.; Klonos, P.A.; Kyritsis, A.; Tarani, E.; Chrissafis, K.; Mašek, O.; Tsachouridis, K.; Anastasiou, A.D.; Bikiaris, D.N. Synthesis and Characterization of PLA/Biochar Bio-Composites Containing Different Biochar Types and Content. *Polymers (Basel).* **2025**, *17*, doi:10.3390/polym17030263.
54. Zouari, M.; Devallance, D.B.; Marrot, L. Effect of Biochar Addition on Mechanical Properties, Thermal Stability, and Water Resistance of Hemp-Polylactic Acid (PLA) Composites. *Materials* **2022**, *15*, doi:10.3390/ma15062271.
55. Hambleton, A.; Fabra, M.J.; Debeaufort, F.; Dury-Brun, C.; Voilley, A. Interface and Aroma Barrier Properties of Iota-Carrageenan Emulsion-Based Films Used for Encapsulation of Active Food Compounds. *J. Food Eng.* **2009**, *93*, 80–88, doi:10.1016/j.jfoodeng.2009.01.001.
56. Quiles-Carrillo, L.; Montanes, N.; Garcia-Garcia, D.; Carbonell-Verdu, A.; Balart, R.; Torres-Giner, S. Effect of Different Compatibilizers on Injection-Molded Green Composite Pieces Based on Polylactide Filled with Almond Shell Flour. *Compos. B Eng.* **2018**, *147*, 76–85, doi:10.1016/j.compositesb.2018.04.017.

 doi:10.20944/preprints202603.1582.v1

57. Gomez-Caturla, J.; Ivorra-Martinez, J.; Tejada-Oliveros, R.; Moreno, V.; Garcia-Garcia, D.; Balart, R. Effect of the Chain Length of Geraniol Esters on the Plasticization Efficiency with Poly(Lactide). *Polymer (Guildf).* **2024**, *290*, 126522, doi:10.1016/j.polymer.2023.126522.
58. Gomez-Caturla, J.; Lascano, D.; Montanes, N.; Balart, R.; Dominici, F.; Puglia, D.; Torre, L. Manufacturing and Characterization of Highly Environmentally-Friendly Composites with Polylactide Matrix and Mango Kernel Seed Flour. *Express Polym. Lett.* **2023**, *17*, 334–351, doi:10.3144/expresspolymlett.2023.24.
59. Tsai, W.-T.; Lin, Y.-Q.; Huang, H.-J. Valorization of Rice Husk for the Production of Porous Biochar Materials. *Fermentation* **2021**, *7*, 70, doi:10.3390/fermentation7020070.
60. Nigiz, F.U.; Özyörü, Z.İ.; Balci, S. Improved Packaging Performance of Olive Tree-Based Biochar-Loaded Poly(Lactic Acid) Films. *Bulgarian Chemical Communications* **2024**, *56*, 352–357, doi:10.34049/bcc.56.3.FUN-M.
61. Balart, J.F.; Montanes, N.; Fombuena, V.; Boronat, T.; Sánchez-Nacher, L. Disintegration in Compost Conditions and Water Uptake of Green Composites from Poly(Lactic Acid) and Hazelnut Shell Flour. *J. Polym. Environ.* **2018**, *26*, 701–715, doi:10.1007/s10924-017-0988-3.